FULL PAPER

Perylene-grafted Silicas: Mechanistic Study and Applications in Heterogeneous Photoredox Catalysis

Adela I. Carrillo,[a],† Ayda Elhage,[a] M. Luisa Marin[a],[b],* and Anabel E. Lanterna[a],*

Abstract: We present here a mechanistic study for the use of heterogeneous photocatalysts based on perylene moieties. First, we show the successful immobilization of perylene diimides (PDI) onto silica matrices, including their full characterization by means of electronic microscopy, surface area measurements, powder XRD, TGA, and FT-IR, ^{29}Si and ^{13}C solid-state NMR, fluorescence and diffuse reflectance spectroscopies. Then, we test the photoredox activity of the material using two model reactions, alkene oxidation and 4-nitrobenzylbromide reduction, and perform mechanistic studies. The mechanistic insights of their photoredox activity show they have promising dual-photocatalytic activity for both organic oxidations and reductions.

Introduction

The future development of chemistry entails environmentally-friendly and energy-sustainable alternatives for organic transformations. Visible light photocatalysis can address these challenges, as reflected by recent numerous reports.[1] Additionally, heterogeneous photocatalysis provides both easy separation of catalyst and light-induced selective organic transformations.[1e, 2]

Perylenes are a family of fluorescent molecules that have been used as pigments, colorants, photoreceptors, and, more recently, as electronic materials because of their characteristic combination of thermal- and photo-stability with optical and redox properties.[3] However, owning the intrinsic insolubility of perylenes, their use as photocatalysts in homogeneous phase usually requires novel designs of perylene derivatives that are soluble in the desired solvent.[4] For instance, Icli *et al.*[5] have shown that engineered modifications of perylene diimides (PDI) can improve solubility in organic solvents; nevertheless, different substituents are necessary to work in higher polar media (*e.g.*, CH_3CN, CH_3OH). Additionally, heavy aggregation is also undesirable due to PDI self-quenching.[6] To overcome this problem, the use of perylene moieties grafted to mesoporous silicas provides a way to fix the sensitizer in place while performing heterogeneous photocatalysis. The use of mesoporous silicas as catalyst supports is an interesting approach due to their interesting structural properties – tuneable pore diameter, large surface areas, high pore volumes, and narrow pore-size distributions.[7] Silica has no inherent catalytic property but can be used as a support functionalized either by framework substitution or by post-synthetic surface modifications;[8] for instance, grafting perylene diimides.[9] These silica-supported sensitizers (PDI-silica) allow easy catalyst separation and excellent catalyst recovery.[3d, 10] Additionally, studies suggest the perylene-grafted silicas retain some emission properties, and they can be quenched in the presence of amines[9] – making them suitable for photoredox catalysis. Despite all these advantages, the use of PDI-silica as photoredox catalysts is virtually unexplored. Therefore, we show here mechanistic studies for the use of these materials in both oxidations and reductions of organic molecules. We start our analysis by studying the photochemical properties of a heterogeneous catalyst prepared by grafting PDI moiety into mesoporous silicas. We show the generation of singlet oxygen ($^1O_2$) by photosensitization of the material under visible light excitation, and prove the versatility of the material to activate photoredox processes. For that, we have selected two model reactions, *i.e.*, oxidations of alkenes into aldehydes and reduction of 4-nitrobenzyl bromide.[11] Finally, we propose a rational mechanism for both oxidation and reduction pathways.

Results and Discussion

Material characterization

We use two different mesoporous silicas, MCM-41 and SBA-15, as supports to immobilize the PDI (see experimental section). The hybrid materials, PDI-MCM and PDI-SBA, are characterized by means of TEM, N_2 adsorption/desorption isotherms, powder XRD patterns, TGA, and FT-IR, ^{29}Si and ^{13}C solid-state NMR, fluorescence and UV-Vis spectroscopies, confirming the grafting of the PDI on the silica materials (see SI).

Structural features of the PDI-MCM and PDI-SBA materials are analysed using microscopic techniques. TEM pictures (Figure 1, top) reveal that after their functionalization with PDI the hexagonal porous arrangement typical of the silica (SBA-15) is maintained (see also Figure S1 for PDI-MCM).

The textural properties of the synthesized materials are evaluated by N_2 adsorption/desorption isotherms (Table 1). As expected, in all cases both the surface area and the mesopore volume decrease after the incorporation of the anchored PDI into the mesopores.[12] TGA analyses reveal that the amount of PDI grafted to the silica is around 0.7 and 0.6 mmol/g of catalyst for PDI-SBA and PDI-MCM, respectively. Powder XRD patterns are also in agreement with maintenance of the hexagonal order of the mesopores after incorporating the PDI moiety (Figure S2).

[a] Dr. Adela I. Carrillo, Dr. Ayda Elhage, Prof. Dr. M. Luisa Marin, Dr. Anabel E. Lanterna
Department of Chemistry and Biomolecular Sciences
Centre for Catalysis Research and Innovation
University of Ottawa
10 Marie Curie, Ottawa K1N 6N5, Canada.
E-mail: marmarin@qim.upv.es; anabel.lanterna@icloud.com
[b] Prof. Dr. M. Luisa Marin
Instituto de Tecnología Química UPV-CSIC
Universitat Politècnica de València
Consejo Superior de Investigaciones Científicas
Avenida de los Naranjos s/n, 46022 Valencia, Spain
[†] As for the author Adela I. Carrillo, the views expressed are purely those of the author and may not be regarded as stating an official position of the European Commission]

Supporting information for this article is given via a link at the end of the document.

The presence of the PDI in the hybrid materials is also verified by using spectroscopic techniques. Figure S3 shows the FT-IR spectra of PDI, MCM-41, SBA-15; together with PDI-MCM and PDI-SBA hybrid materials. In all samples, bands observed at 1200, 1040 and 800 cm^{-1} are attributed to Si-O-Si vibrations and the shoulder that appears at 960 cm^{-1} corresponds to the Si-OH vibration.[13] Hybrid materials and the PDI also show the characteristic peaks of the perylene moiety, *i.e.*, peaks at 1695 and 1655 cm^{-1} due to the vibrations of the C=O groups and the peak around 1595 cm^{-1} resulting from various vibrations of the perylene aromatic core.[14]

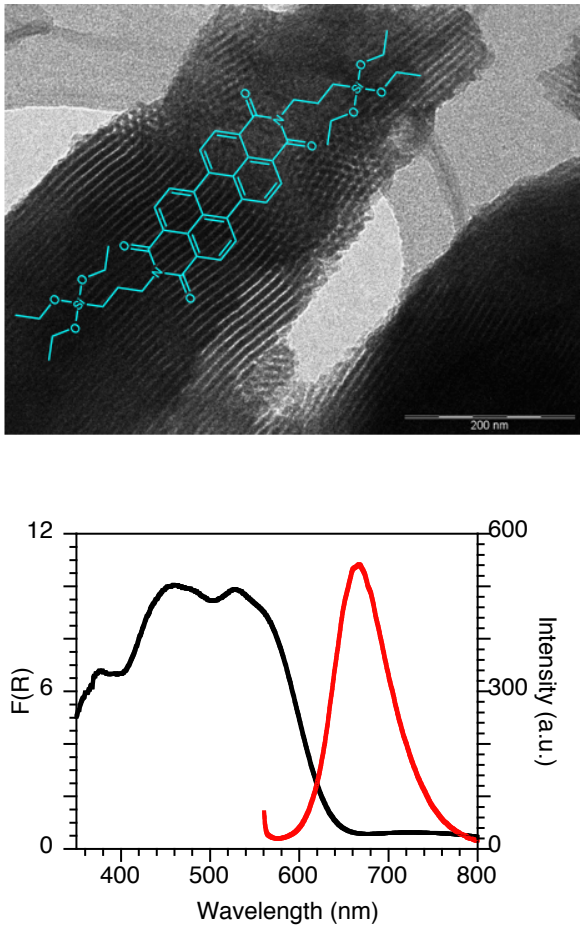

Figure 1. Top: TEM images of the hybrid PDI-SBA. PDI structure is shown in cyan. **Bottom**: DR (black) and fluorescence (red) spectra of the PDI-SBA hybrid material.

Table 1. Textural properties of the PDI-silicas.

Sample	A_{BET}[a] (m^2/g)	V_p^{BJH}, [b] (cm^3/g)
MCM-41	628.0	0.22
PDI-MCM	233.2	0.03
SBA-15	670.1	0.69
PDI-SBA	229.0	0.24

[a]The Brunauer-Emmett-Teller (BET) surface area was estimated by multipoint BET method using the adsorption data in the relative pressure (P/P_0) range of 0.05-0.3. [b]Mesopore volume from the isotherms at the relative pressure of 0.8.

The effective incorporation of the PDI onto the mesoporous silica materials is also supported by solid-state NMR spectroscopy. Figures S4-S6 show the ^{29}Si and ^{13}C NMR spectra of PDI and PDI-SBA (same as PDI-MCM). ^{29}Si NMR shows two groups of signals, the first one, between -92 and -110 ppm, confirms the presence of the silica framework,[8a] thus the only signals present in the silica matrix (SBA-15 or MCM-41),[15] and the second group, between -45 and -70 ppm, acts as a confirmation of the covalent linkage of the PDI [T^m = perylene-$Si(OSi)_m(OH)_{3-m}$, m = 2-3].[16] Furthermore, ^{13}C signals found in the PDI-SBA sample are in agreement with the PDI ^{13}C NMR spectrum.

Finally, the UV-Vis diffuse reflectance (DR) and fluorescence spectra of the PDI-silicas (solid state measurements) show the same profile regardless the nature of the silica (Figure 1, bottom). Likewise, excitation wavelengths ranging from 400 to 600 nm were employed to obtain emission spectra centred at *ca.* 660 nm, regardless of the excitation wavelength employed.

Sensitized singlet oxygen formation

PDI-silicas are expected to generate $^1O_2$ upon excitation, as the PDI does in solution (see Fig. S7). Fluorescence quantum yields of perylenes are reported to be higher than 0.97.[17] In addition, singlet and triplet energies are *ca.* 54 and 27 $kcalmol^{-1}$, respectively.[18] This singlet-triplet energy gap allows formation of singlet oxygen from the singlet excited state.[19] In fact, the efficiency of the $^1O_2$ production from perylene singlet states is reported as 0.27 in acetonitrile.[20] To investigate the formation of $^1O_2$ in the case of the heterogeneous materials, we select a chemical method, specifically, the oxidation of 9,10-dimethylanthracene (DMA) to its corresponding endoperoxide (see SI).[13, 21] DMA exhibits distinct absorption bands between 310 and 410 nm, which are not obscured by PDI-silicas (Figure S8), and thus can be easily monitored by UV-Vis spectroscopy. Thus, selective excitation of PDI-silicas under visible light excitation, in the presence of DMA under oxygen atmosphere was performed. The consumption of DMA was monitored at 377 or 398 nm and the kinetics of the reaction was fitted to a pseudo-first order model (See SI).

The dependence of k_{obs} obtained for PDI-silicas and also for PDI in homogeneous solutions at different PDI concentrations, is shown in Figure S9. As it is usual for both homogeneous and heterogeneous catalytic systems, the rate increases linearly with the photocatalyst concentration, because of the increase in the

absorbed photon flux. It is expected that the rate of the reaction reaches a region where it stays constant, thus a region representing concentrations of constant and optimal light absorption. Note that due to the low solubility of PDI in the current solvent, such region can only be reached when PDI is grafted to the silicas. Thus, the amount of sensitizer that can be used is higher in the cases of PDI-silicas. Indeed, when PDI-SBA is used, we can observe the rate reaches a plateau at ca. $7x10^{-3}$ s^{-1}. Also, we note that the PDI reactivity remains the same in homogeneous phase and in SBA when comparing the same PDI concentration (~ 10 μM region). This shows that grafting PDI into silicas can retain the PDI intrinsic catalytic activity, adding the advantages of ease of separation and reusability (*vide infra*). Finally, it is worth mentioning that the higher catalytic activity of PDI-SBA compared to PDI-MCM can be rationalized in terms of the lower particle size of PDI-SBA, that allows the photocatalyst to remain in suspension more easily. SEM imaging (Figure S10) of the two different silicas clearly shows different particle sizes, which agrees with the lower stability of the PDI-MCM suspensions.

In order to compare the activity of the two PDI-silicas, the same experiment is carried out preparing suspensions with similar absorption spectra (Figure S11). The values of k_{obs} obtained for PDI-silicas and also for PDI in homogeneous solutions –or their physical mixtures– are shown in Table 2. As it is expected, the same reaction rate is found for cases were PDI is in solution or physically mixed to silicas. Noticeably, the PDI-SBA shows the greatest rate constant, therefore it was selected for further studies.

Table 2. k_{obs} for the oxidation of DMA by $^1O_2$, using PDI in homogeneous and in heterogeneous conditions.

Entry	Photosensitizer	k_{obs} (10^{-4} s^{-1})
i	PDI	18.3
ii	PDI-MCM	6.5
iii	PDI-SBA	60
iv	MCM + PDI	22
v	SBA + PDI	16

LED current: 1A. λ_{max}: 530 nm. Irradiance: 0.27 W cm^{-2}. Cut on filter: 500 nm. [DMA] = 23 μM. All suspensions present similar absorption spectra (See Figure S11).

Moreover, since PDI-SBA and PDI-MCM show broaden absorption spectra than the parent PDI, we also test the generation of $^1O_2$ using different excitation wavelengths as shown in Figure 2 top. For this, we use the same amount of PDI (~10 μM) in solution and in the PDI-SBA suspension. The results in table 3 suggest that PDI-SBA can take advantage of a broaden region of the visible spectrum, and are better illustrated in Figure 2 bottom.

Table 3. k_{obs} for the oxidation of DMA by $^1O_2$, using PDI in homogeneous and in heterogeneous conditions upon different excitation wavelengths.

Entry	Photosensitizer	λ_{max}	k_{obs} (10^{-4} s^{-1})
i	PDI-SBA	465[a]	22.9
ii	PDI-SBA	530[b]	17.8
iii	PDI-SBA	590[b]	6.2
iv	PDI	465[a]	6.5
v	PDI	530[b]	18.6
vi	PDI	590[b]	<<1

Irradiation power: ~0.36 W cm^{-2}. [a]Cut on filter: 460 nm. [b]Cut on filter: 500 nm. Notice all samples have same PDI concentration (~10 μM).

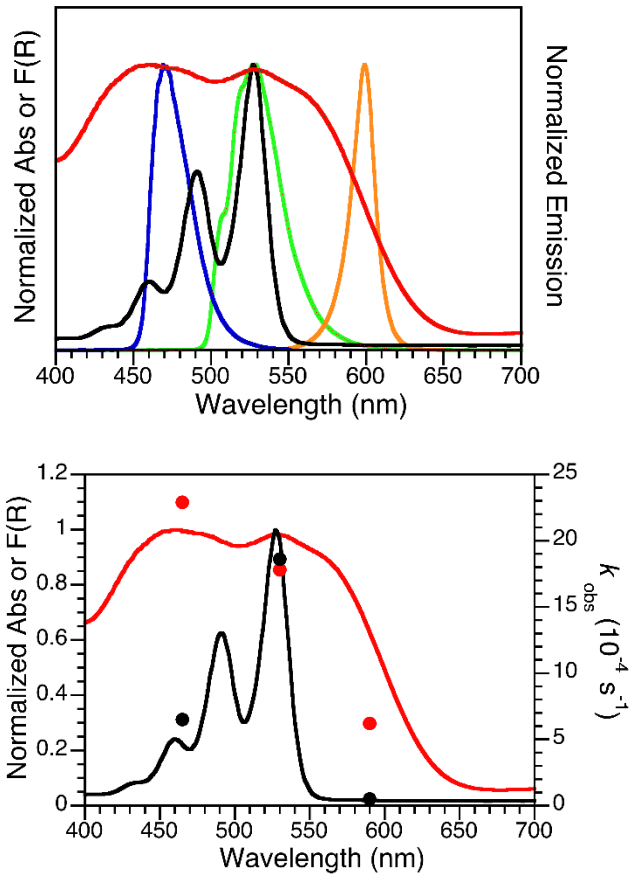

Figure 2. Top: Normalized absorption spectra of PDI (black) and PDI-SBA (red); and normalized emission spectra of 465 nm LED (blue), 530 nm LED (green) and 590 nm LED (orange). **Bottom**: Normalized absorption spectra of PDI (black) and PDI-SBA (red); and k_{obs} at different excitation wavelengths (see Table 3).

Additionally, we test the reusability of PDI-SBA using the same conditions described in table 2. Once the DMA was completely consumed, the same amount of DMA was added to the suspension and the evolution of the reaction was followed again. After 5 cycles we observed the same reaction rate, suggesting the photocatalyst capacity to generate $^1O_2$ is maintained. Further, no leaching PDI was found after reaction, thus the silica-supported PDI act as real heterogeneous photocatalysts.

Electron transfer photocatalytic oxidation

PDI compounds are also believed to undergo reductive photoredox catalytic cycles. In particular our PDI shows a redox potential value ($E_{1/2}$ ($PDI^{\bullet-}$/PDI) *vs* Fc/Fc^+ = -0.95 V (-0.57 V *vs* SCE)) in agreement with those reported for related perylenes.[22] Upon excitation, both reductive and oxidative properties of PDI are enhanced[1d] and therefore, PDI excited state (PDI*) can experience an electron transfer process with common electron donors, such as amines, forming a PDI radical anion ($PDI^{\bullet-}$, $E_{1/2}$ ($PDI^{\bullet-}$/PDI*) *vs* SCE = +1.77 V). The presence of this species is easily detected by UV-vis spectroscopy due to the characteristic absorption band of $PDI^{\bullet-}$ around 700 nm. To prove this, we have irradiated the PDI precursor in solution in the presence of an amine (*e.g.*, triethylamine –TEA). Figure 3A shows the formation of the $PDI^{\bullet-}$ upon 530 nm LED excitation and its quenching in the presence of O_2. Accordingly, the formation of the $PDI^{\bullet-}$ species is also demonstrated by using the PDI-SBA material (Figure 3B).

Photocatalytic applications

Based on the versatile properties of PDI, specifically on its capability of generating $^1O_2$, and also on its potential as a reducing agent from its first singlet excited state, we envision that two opposite yet complementary redox reactions can be tested in the presence of heterogeneous PDI-SBA. Therefore, we select two test reactions as “proof of concept”: the oxidation of stilbenes and the reduction of 4-nitrobenzylbromide (4-NBB), summarized in Scheme 1. Notice that our examples use single-photon excitation, *i.e.*, using any of the light sources shown in Figure 2 top, only PDI species is excited as opposed to previous studies where excitation of $PDI^{\bullet-}$ (λ_{abs} between ~650-850 nm, see Figure 3) was suggested.[11a]

The oxidative scission of stilbenes to form aldehydes has been performed using expensive homogeneous Ru complexes and co-oxidants such as $NaIO_4$.[23] In our preliminary screening of conditions, we find that PDI-SBA can catalyse this reaction for different *p*-substituted *t*-stilbenes (Table S1) in a more environmentally-friendly process, using green light excitation, molecular oxygen as oxidant, and heterogeneous conditions.[1c] On the other hand, the reduction of 4-NBB is easily achieved by green LED light irradiation of a catalyst suspension in CH_2Cl_2 under Ar atmosphere, using an amine as a sacrificial electron donor (Table S2).

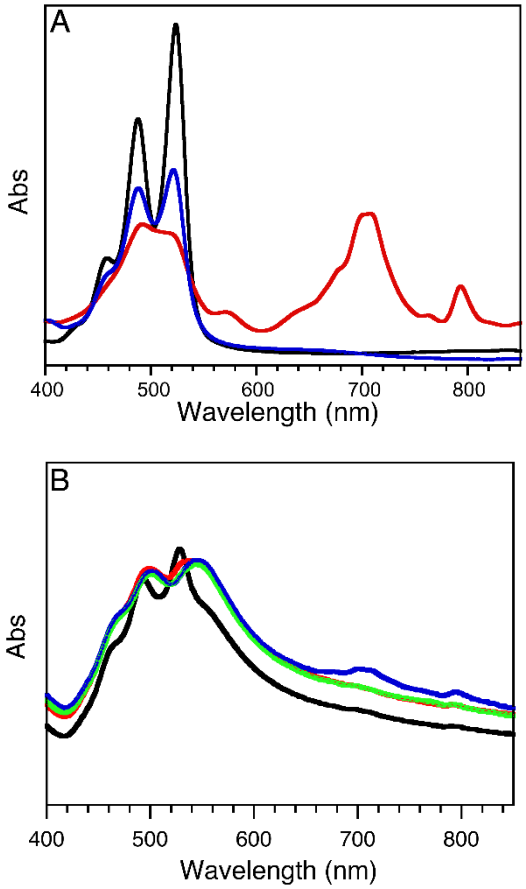

Figure 3. A: UV-vis absorption spectra of PDI in DMF in the presence of TEA (100 mM) under Ar atmosphere in the dark (black) and upon 2 min irradiation (red) with a 530 nm LED. Notice the formation of the characteristic absorption band for $PDI^{\bullet-}$ around 700 nm. $PDI^{\bullet-}$ disappears quickly upon addition of O_2 (blue). **B**: Absorption spectra of PDI-SBA suspension in DMF before (black) and after addition of 25 mM TEA (red) under Ar atmosphere. The mixture was irradiated for 5 min with a 465 nm LED (blue) –showing a new band around 700 nm corresponding to $PDI^{\bullet-}$ formation– and then exposed to air (green).

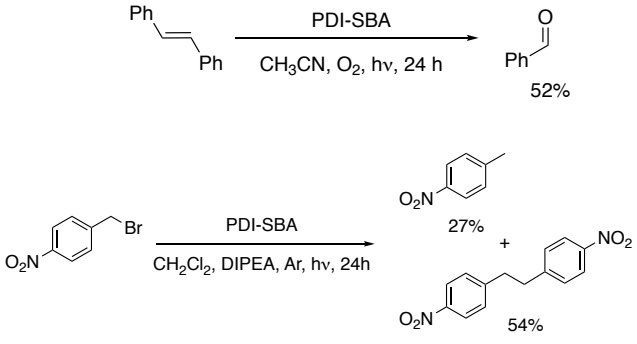

Scheme 1. Model reactions used to test the catalytic activity of PDI-SBA. **Top**: Photocatalytic oxidation of *t*-stilbene. **Bottom**: Photocatalytic reduction of 4-nitrobenzylbromide.

These preliminary results suggest that PDI-SBA material has great potential to catalyse oxidation or reduction reactions, showing versatility to operate under different conditions. We therefore perform different tests in order to understand the mechanism operating under those conditions. Starting from the oxidation process, we propose the mechanism depicted in Scheme 2A, where the singlet excited state (PDI*) can be readily quenched by *t*-stilbene (Table S2) to form the coloured radical anion $PDI^{\bullet-}$ as shown in Figure 4A. Subsequent quenching of the radical cation derived from *t*-stilbene by O_2, $^1O_2$ or $O_2^{\bullet-}$ leads to oxidation products (Table S1). Additionally, we also prove that $PDI^{\bullet-}$ can be quenched by O_2 (Figure 3A), more likely forming reactive oxygen species.

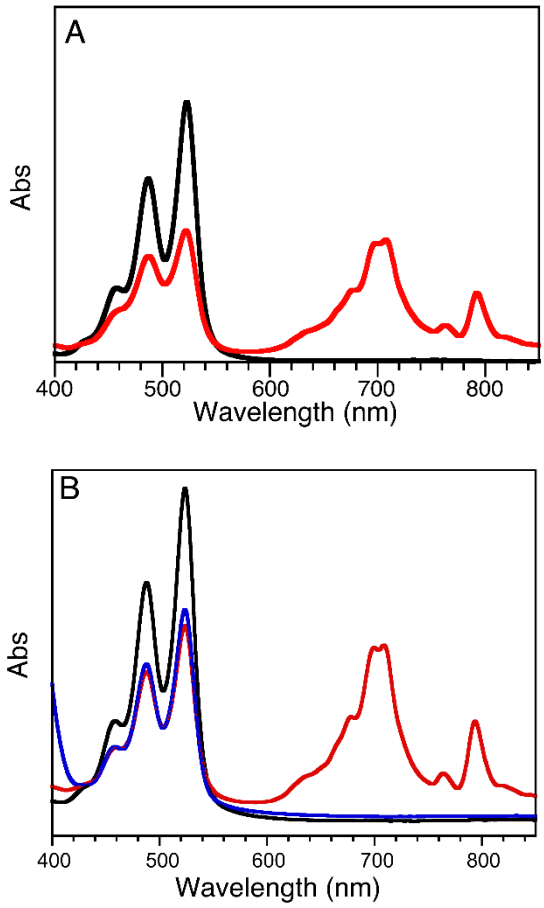

Figure 4. A: UV absorption spectrum of PDI in DMF in the presence of stilbene (20 mM) under Ar atmosphere in the dark (black) and upon 5 min irradiation (red) with a 465 nm LED. Notice the formation of the characteristic absorption band for $PDI^{\bullet-}$ around 700 nm. **B**: UV-vis absorption spectra of PDI in DMF in the presence of TEA (100 mM) under Ar atmosphere in the dark (black) and upon 2 min irradiation (red) with a 530 nm LED. Notice the formation of the characteristic absorption band for $PDI^{\bullet-}$ around 700 nm. $PDI^{\bullet-}$ disappears quickly upon addition of 25 mM of 4-NBB (blue).

In the case of the reduction of 4-NBB, a plausible mechanism (Scheme 2B) involves the excitation of PDI to its singlet-excited state (PDI*) followed by the injection of an electron from a sacrificial electron donor (SED), *e.g.*, an amine (Table S2). This was confirmed by the formation of the $PDI^{\bullet-}$ which can be restored to the original PDI ground state by interaction with 4-NBB, leading to the formation of benzyl radical. This is supported by the quick disappearance of the $PDI^{\bullet-}$ visible band upon addition of 4-NBB (Figure 4B). The reaction would compete with quenching from O_2 and therefore, it needs to be performed under deaerated conditions.

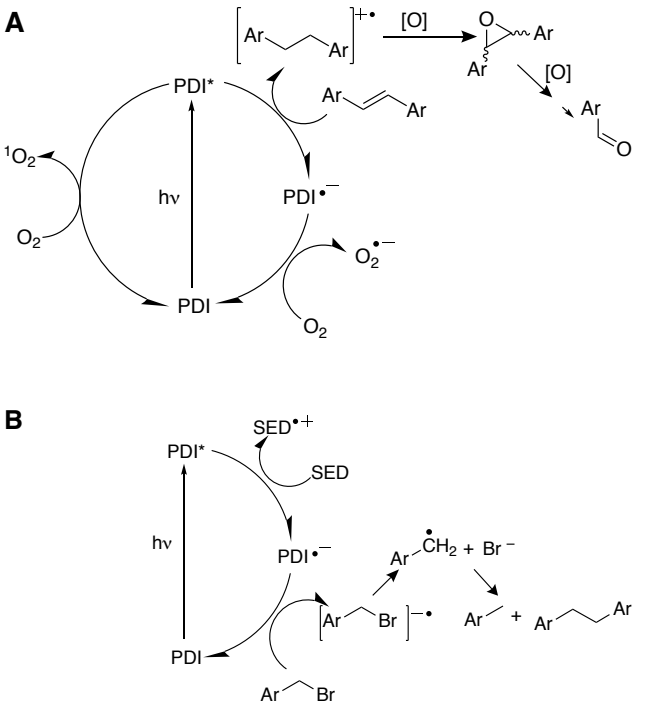

Scheme 2. A: Proposed mechanism for the photocatalytic oxidation of stilbenes (Ar = phenyl). Note that [O] could be O_2, $^1O_2$ and/or $O_2^{\bullet-}$. **B**: Proposed mechanism for the photocatalytic reduction of benzyl bromides (Ar = 4-nitrophenyl). SED: sacrificial electron donor.

Conclusions

In summary, we show the mechanism of action of perylene diimide moiety grafted onto silica supports as versatile heterogeneous photoredox catalysts. These PDI-silicas can readily act as sensitizers for single oxygen formation, favouring the dispersion of a greater amount of sensitizer in the suspensions compared to the homogeneous PDI solutions. The appeal of the material lies on its photocatalytic activity for both oxidation and reduction transformations under mild reaction conditions, along with the ease of separation and potential reusability. In particular, the oxidative scission of stilbenes can be performed under visible light and using only O_2 (at atmospheric pressure) as oxidant. In the case of the reduction of 4-nitro-benzyl bromide, we find 81% total yield, which accounts for both dimer

and reductive products, under argon atmosphere in the presence of amines as sacrificial electron donors. Finally, he mechanistic studies for both oxidation and reduction processes can pave the way to further study the versatility of this material with other organic photoredox transformations.

Experimental Section

Materials

Tetraethylorthosilicate (TEOS, 98%) was used as silica precursor. Cetyltrimethylammonium bromide (CTAB, 96%), and pluronic (P123) were used as structure-directing agents. Aqueous ammonia solution (NH_4OH, 30%) and hydrochloric acid were also used in the synthetic protocol to obtain the final mesoporous materials. Perylene-3,4,9,10-tetracarboxylic dianhydride (PTCD) and 3-aminopropyltriethoxysilane (APTES) were used to synthesize the perylene derivative (PDI) to be anchored to the mesoporous silica materials. 9,10-dimethylanthracene (DMA), *t*-stilbene, *t*-stilbene oxide, 4-nitrobenzyl bromide (4-NBB), triethylamine (TEA), diisopropylethylamine (DIPEA) were purchased from Sigma-Aldrich and used as received.

Synthesis of perylene diimide (PDI)

PDI was synthesized by modifying a reported protocol.[7b] Briefly, 2 g of PTCD were purged with N_2 in a round bottom flask. Then, 4 mL of APTES were added and the reaction mixture was stirred for 20 h under N_2 atmosphere at 150 ºC in the dark. After cooling to room temperature, the dark red solid was placed into a Soxhlet system and washed for a week with petroleum ether to remove the excess of APTES. Then, acetone was used to extract the residue. The solvent was then slowly evaporated by using a rotary evaporator to afford the desired PDI product.

Synthesis of perylene-grafted silicas (PDI-silicas)

Mesoporous silica (0.2 g), MCM-41 or SBA-15, prepared by published methods,[6a] were dehydrated in an oven at 200 ºC for 2 h. Then, 50 mL of anhydrous toluene was added to the activated materials and this mixture was stirred for 1 h in order to obtain a well dispersed suspension. Finally, 0.32 g of the PDI were added to the reaction mixture and refluxed overnight. The obtained red PDI-silica solid was filtered, washed with fresh toluene and acetone and air-dried. In a final step the solid was placed into a Soxhlet system and was washed with acetone for 2 days to remove the un-reacted PDI.

Characterization

Transmission electron microscopy (TEM) images were collected with a Philips CM-10 microscope operating at 100 kV. Scanning electron microscopy (SEM) images were acquired on JSM-7500F FESEM (JEOL) microscope, working voltage: 20 kV. The textural properties of the solids (degassed for 4 h at 373 K at 5 x 10-5 bar) were determined from N_2 adsorption at 77 K in an AUTOSORB-6 apparatus. The pore size distribution was determined from the Barret-Joyner-Helender (BJH) method applied to the adsorption branch of the obtained isotherms. The surface area was determined using the multipoint BET method in the 0.05-0.30 relative pressure ranges. Mesopore volume was measured at the plateau of the adsorption branch of the nitrogen isotherm, P/Po = 0.8. Thermogravimetric analysis (TGA) was collected on a TA Instruments Q5000 IR Thermogravimetric Analyzer. Small-angle powder XRD analysis was carried out with a Rigaku Ultima IV diffractometer using a CuKa radiation (k = 1.541836 A), operating at 40 kV and 44 mA, at a scanning velocity of 0.25 deg/min in the $0.7 < 2\theta < 10$ range. FT-IR was collected on a Thermo Nicolet NEXUS 670 FT-IR instrument. Solid-state NMR spectra were recorded at room temperature under magic angle spinning (MAS) in a Bruker AV-400 spectrometer using a BL-4 probe with 4 mm diameter zirconia rotors spinning at 10 kHz. ^{1}H to ^{13}C CP/MAS NMR spectra were measured at 100.61 MHz and recorded with proton decoupling. ^{29}Si MAS NMR spectra were measured at 79.46 MHz. The ^{13}C and ^{29}Si spectra were referred to adamantane (CH_2 signal at 38.3 ppm) and TMS (0 ppm), respectively.

UV-visible spectra were recorded using a Cary 100 spectrometer. For diffuse reflectance (DR) spectra the same spectrometer equipped with a Labsphere Inc. DRA-30I diffuse reflectance accessory was used. Fluorescence spectra of PDI solutions were obtained with a Photon Technology International (PTI) spectrofluorimeter at room temperature. Fluorescence lifetimes were measured in an Easy-Life (from PTI) system using a 530 nm LED pulse excitation and the lifetimes calculated in the Easy-Life integrated software. Fluorescence spectra of solid samples were acquired with a LS50 Perkin Elmer spectrofluorimeter. Singlet Oxygen detection was carried out in a Laser flash photolysis system (LFP 111 system, Luzchem Inc., Ottawa, Canada) using a 532 nm excitation pulse generated with a Nd-YAG laser operating at 10 mJ/pulse.

Electrochemical measurements were carried out using a computer-controlled potentiostat Autolab/PGSTAT 101 (Eco-Chimie) with NOVA software. A three-electrode electrochemical cell was employed for the electrochemical measurements. The working, counter, and pseudo-reference electrodes were glassy carbon electrodes with diameters of 2 mm, and Pt-wire electrodes, respectively. The potentials were measured with respect to ferrocene couple (Fc/Fc^+) at room temperature in an Eppendorf cup degassed with Ar using 0.5 mL of 1-Butyl-3-methylimidazoliumtriflate. Scan rate: 0.2 V/s.

Chemical detection of singlet oxygen formation

The photooxygenation of 9,10-dimethylanthracene (DMA) was carried out in the presence of PDI, PDI-MCM or PDI-SBA in a mixture ethanol/water 90:10 at 293 K using a single LED working at 1000 mA with a maximum emission at 530 nm. The incident light was filtered in order to cut out light below 500 nm and eliminate any direct photochemical reaction of DMA. The initial concentration of DMA was 23.3 μM, and its concentration was measured by UV spectroscopy, following the decrease of the 377 nm or 398 nm band.

Photocatalytic activity

Photoredox reactions were performed using a light-emitting diode system (LED) consisted of four, 10 W 530 nm LedEngin LZ4-40G110 emitters attached to aluminum heat sinks in a custom design irradiator using a thermal bath with water/ethanol circulation for temperature control (set T = 5°C). The intensity of each individual emitter at the distance the sample is placed was measured (0.48 W cm^{-2}).

Identification and quantification of the reaction products was performed using a Waters Integrity HPLC in tandem with a reverse phase C18 Zorbax column or a Perkin Elmer GC coupled with a FID or Mass detector, and the NMR spectrometer Bruker Avance II 400.

The oxidation of stilbene was performed in aerated CH_3CN by ca. 3 mg of the PDI-SBA, 15 mg of stilbene with green LED irradiation for around 20 h. Reaction progress was followed by GC-MS while quantification of products was analyzed by CG-FID using naphthalene as external standard.

The reduction of 4-NBB was carried out using ca. 4.5 mg of the PDI-SBA, 20 mg of 4-NBB (0.09 mmol) and 2 eq. of the DIPEA in 5 mL of strictly deaerated dichloromethane. The reaction was irradiated with green LEDs for 5 or 24 h. The reaction was analyzed by ^{1}H NMR and quantified using caffeine as external standard.

Acknowledgements

This work was supported by the Natural Sciences and Engineering Research Council of Canada, and the Canada Foundation for Innovation. The authors are grateful to Prof. J. C. Scaiano for his generous support.

Keywords: heterogeneous catalysis • MCM-41 • photoredox catalysis • reaction mechanisms • SBA-15

[1] a) L. Marzo, S. K. Pagire, O. Reiser and B. Konig, *Angew. Chem., Int. Ed.* **2018**, *57*, 10034-10072; b) M. A. Miranda and M. L. Marin, *Green and Sustainable Chemistry* **2017**, *6*, 139-149; c) T. P. Yoon, *Acc. Chem. Res.* **2016**, *49*, 2307-2315; d) S. P. Pitre, C. D. McTiernan and J. C. Scaiano, *Acc. Chem. Res.* **2016**, *49*, 1320-1330; e) X. Lang, X. Chen and J. Zhao, *Chem. Soc. Rev.* **2014**, *43*, 473-486; f) D. M. Schultz and T. P. Yoon, *Science* **2014**, *343*, 1239176; g) C. K. Prier, D. A. Rankic and D. W. C. MacMillan, *Chem. Rev.* **2013**, *113*, 5322-5363; h) J. M. R. Narayanam and C. R. J. Stephenson, *Chem. Soc. Rev.* **2011**, *40*, 102-113.

[2] a) J. C. Colmenares and Y. J. Xu, *Heterogeneous photocatalysis from fundamentals to green applications*, Springer, Berlin, **2016**; b) S. Sarina, E. R. Waclawik and H. Zhu, *Green Chemistry* **2013**, *15*, 1814-1833; c) Y. Q. Qu and X. F. Duan, *Chem. Soc. Rev.* **2013**, *42*, 2568-2580; d) J. X. Jiang, Y. Li, X. Wu, J. Xiao, D. J. Adams and A. I. Cooper, *Macromolecules* **2013**, *46*, 8779-8783; e) M. A. Fox and M. T. Dulay, *Chem. Rev.* **1993**, *93*, 341-357.

[3] a) H. L. Sun, L. Wang, Y. F. Wang and X. G. Guo, *Chem. Eur. J.* **2019**, *25*, 87-105; b) A. Nowak-Krol, K. Shoyama, M. Stolte and F. Wurthner, *Chem. Commun.* **2018**, *54*, 13763-13772; c) E. Arzoumanian, F. Ronzani, A. Trivella, E. Oliveros, M. Sarakha, C. Richard, S. Blanc, T. Pigot and S. Lacombe, *ACS Appl. Mater. Interfaces* **2014**, *6*, 275-288; d) S. Mathew and H. Imahori, *J. Mater. Chem.* **2011**, *21*, 7166-7174; e) Y. Wu, Y. Zhen, Y. Ma, R. Zheng, Z. Wang and H. Fu, *J. Phys. Chem. Lett.* **2010**, *1*, 2499-2502; f) F. Würthner, *Chem. Commun.* **2004**, 1564-1579; g) S. Ferrere and B. A. Gregg, *New J. Chem.* **2002**, *26*, 1155-1160.

[4] a) F. J. Cespedes-Guirao, A. B. Ropero, E. Font-Sanchis, A. Nadal, F. Fernandez-Lazaro and A. Sastre-Santos, *Chem. Commun.* **2011**, *47*, 8307-8309; b) F. J. Cespedes-Guirao, L. Martin-Gomis, K. Ohkubo, S. Fukuzumi, F. Fernandez-Lazaro and A. Sastre-Santos, *Chem. Eur. J* **2011**, *17*, 9153-9163.

[5] a) J. B. Bodapati and H. Icil, *Dyes and Pigments* **2008**, *79*, 224-235; b) G. Türkmen, S. Erten-Ela and S. Icli, *Dyes and Pigments* **2009**, *83*, 297-303.

[6] F. X. Zhang, Y. S. Ma, Y. H. Chi, H. H. Yu, Y. N. Li, T. Y. Jiang, X. F. Wei and J. M. Shi, *Sci. Rep.* **2018**, *8*, 11.

[7] a) A. Taguchi and F. Schuth, *Microporous Mesoporous Mater.* **2005**, *77*, 1-45; b) D. T. On, D. Desplantier-Giscard, C. Danumah and S. Kaliaguine, *Appl. Catal. A* **2001**, *222*, 299-357.

[8] a) A. I. Carrillo, J. Garcia-Martinez, R. Llusar, E. Serrano, I. Sorribes, C. Vicent and J. A. Vidal-Moya, *Microporous Mesoporous Mater.* **2012**, *151*, 380-389; b) J. Garcia-Martinez, N. Linares, S. Sinibaldi, E. Coronado and A. Ribera, *Microporous Mesoporous Mater.* **2009**, *117*, 170-177.

[9] a) D. Sriramulu, S. P. Turaga, A. A. Bettiol and S. Valiyaveettil, *Sci. Rep.* **2017**, *7*; b) M. A. Wahab, H. Hussain and C. He, *Langmuir* **2009**, *25*, 4743-4750.

[10] F. Ronzani, P. Saint‐Cricq, E. Arzoumanian, T. Pigot, S. Blanc, M. Oelgemöller, E. Oliveros, C. Richard and S. Lacombe, *Photochem. Photobiol.* **2014**, *90*, 358-368.

[11] a) J. T. Shang, H. Y. Tang, H. W. Ji, W. H. Ma, C. C. Chen and J. C. Zhao, *Chinese J. Catal.* **2017**, *38*, 2094-2101; b) A. E. Lanterna, A. Elhage and J. C. Scaiano, *Catal. Sci. Technol.* **2015**, *5*, 4336-4340.

[12] D. T. Marquez, A. I. Carrillo and J. C. Scaiano, *Langmuir* **2013**, *29*, 10521-10528.

[13] E. Albiter, S. Alfaro and M. A. Valenzuela, *Photochem. Photobiol. Sci.* **2015**, *14*, 597-602.

[14] V. Prusakova, C. E. McCusker and F. N. Castellano, *Inorg. Chem.* **2012**, *51*, 8589-8598.

[15] R. Simonutti, A. Comotti, S. Bracco and P. Sozzani, *Chem. Mater.* **2001**, *13*, 771-777.

[16] A. Cardelli, L. Ricci, G. Ruggeri, S. Borsacchi and M. Geppi, *Eur. Polym. J.* **2011**, *47*, 1589-1600.

[17] S. Prathapan, S. I. Yang, J. Seth, M. A. Miller, D. F. Bocian, D. Holten and J. S. Lindsey, *The Journal of Physical Chemistry B* **2001**, *105*, 8237-8248.

[18] a) W. E. Ford and P. V. Kamat, *The Journal of Physical Chemistry* **1987**, *91*, 6373-6380; b) M. Ghirotti, C. Chiorboli, C. C. You, F. Wurthner and F. Scandola, *J. Phys. Chem. A* **2008**, *112*, 3376-3385.

[19] A. F. Olea and F. Wilkinson, *J. Phys. Chem.* **1995**, *99*, 4518-4524.

[20] N. J. Turro, V. Ramamurthy and J. C. Scaiano, *Modern Molecular Photochemistry of Organic Molecules*, University Science Publishers, New York, N.Y., **2010**.

[21] F. Wilkinson, W. P. Helman and A. B. Ross, *J. Phys. Chem. Ref. Data* **1993**, *22*, 113-262.

[22] Y. Z. Zhao, K. X. Li, S. Y. Ding, M. Zhu, H. P. Ren, Q. Ma, Z. Guo, S. P. Tian, H. Q. Zhang and Z. C. Miao, *Russ J Phys Chem A* **2018**, *92*, 1261-1265.

[23] a) P. Daw, R. Petakamsetty, A. Sarbajna, S. Laha, R. Ramapanicker and J. K. Bera, *J. Am. Chem. Soc.* **2014**, *136*, 13987-13990; b) E. A. Nyawade, H. B. Friedrich, B. Omondi and P. Mpungose, *Organometallics* **2015**, *34*, 4922-4931; c) S. Muthumari and R. Ramesh, *ChemistrySelect* **2018**, *3*, 3036-3041.